ResearchGate

See discussions, stats, and author profiles for this publication at: https://www.researchgate.net/publication/231236580

Fabrication and Characteristics of Ordered Ni Nanostructures on Glass by Anodization and Direct Current Electrodeposition

ARTICLE *in* CHEMISTRY OF MATERIALS · OCTOBER 2002

Impact Factor: 8.35 · DOI: 10.1021/cm020272w

CITATIONS
102

READS
52

4 AUTHORS, INCLUDING:

Song-Zhu Kure-Chu
Iwate University
48 PUBLICATIONS **1,262** CITATIONS

SEE PROFILE

Available from: Song-Zhu Kure-Chu
Retrieved on: 22 January 2016

Fabrication and Characteristics of Ordered Ni Nanostructures on Glass by Anodization and Direct Current Electrodeposition

Song-Zhu Chu,* Kenji Wada, Satoru Inoue, and Sin-ichi Todoroki

Advanced Materials Laboratory, National Institute for Materials Science, Namiki 1-1, Tsukuba, Ibaraki, 305-0044, Japan

Yukiko K. Takahashi and Kazuhiro Hono

Materials Engineering Laboratory, National Institute for Materials Science, Sengen 1-2-1, Tsukuba, Ibaraki, 305-0047, Japan

Received March 15, 2002. Revised Manuscript Received September 4, 2002

A novel process for fabrication of metal nanostructure arrays directly on glass substrates is described. An aluminum film was sputter-deposited on a glass substrate coated with a tin-doped indium oxide (ITO) film. The films were then anodically oxidized to obtain a porous alumina template, with pore diameters ranging from 5 to 150 nm, which was used as a template-electrode in a direct current electrodeposition to fabricate various nickel nanowires (∅ 18−180 nm, 0.5−2.6 μm long) in the nanopores. The porous alumina films not only define the dimensions of the nanowires but also influence the crystalline orientation. The magnetic hysteresis measurement showed that the Ni nanowire arrays have significant magnetic anisotropy proportional to their aspect ratios. The coercivity (H_c) and the squareness (M_r/M_s) perpendicular to the substrates were 1025 Oe and 0.74 for the Ni nanowires of ∅ 50 nm (1.8 μm), and 830 Oe and 0.94 for the Ni nanowires of ∅ 18 nm (1.2 μm), respectively.

Introduction

Nanostructured materials have attracted great interest in their novel physical and chemical properties different from those in bulk state and in their potential applications for developing new types of electronic, magnetic, optic, photocatalytic, and energy storage devices.[1,2] In particular, the fabrication of metal nanowires has recently attracted much attention because of their unique magnetic properties and other potential technological applications.[3−9] One of the useful techniques to fabricate metal nanowires is the electrodeposition method by which ferromagnetic metals and alloys can be electrochemically deposited into the nanopores of template materials. This method is an inexpensive technique to obtain nanowires with different morphologies controlled by the characteristics of the templates. The commonly used templates are polycarbonate films,[4,5] commercial alumina membranes,[6−9] and porous anodic oxide films produced from pure aluminum plates,[10−13] by which many ferromagnetic nanowires have been successfully prepared.[2−13] Among these, the anodically oxidized alumina films have a greater advantage than the polycarbonate films because of their chemical and thermal stability against annealing. Furthermore, the aluminum anodizing technology has been developed to such a level that not only the pore dimensions but also the distribution and shape of pores in the films can be artificially controlled by means of pre-indentation procedures.[14,15]

The alternating current (AC) electrodeposition of metals in the pores of anodically oxidized aluminum plates has been known for a long time for the purposes of coloring anodic alumina films [16−18] and magnetic recording applications.[10,11,19,20] In AC electrodeposition,

* To whom correspondence should be addressed. Fax: 81-298-54-9060. E-mail: CHU.Songzhu@nims.go.jp.

(1) Martin, C. R. *Science* **1994**, *266*, 1961.
(2) Schwarzacher, W.; Kasyutich, O. I.; Evans, P. R.; Darbyshire, M. G.; Yi, G.; Fedosyuk, V. M.; Rousseaux, F.; Cambril, E.; Decanini, D. *J. Magn. Magn. Mater.* **1999**, *198−199*, 185.
(3) Vázquez, M. *Physics B* **2001**, *299*, 302.
(4) Valizadeh, S.; George, J. m.; Leisner, P.; Hultman, L. *Thin Solid Films* **2002**, *402*, 262.
(5) Ge, S.; Ma, X.; Li, C.; Li, W. *J. Magn. Mater.* **2001**, *226−203*, 1867.
(6) Raposo, V.; Garcia, J. M.; González, J. M.; Vázquez, M. *J. Magn. Magn. Mater.* **2000**, *222*, 227.
(7) Zhang, X. Y.; Zhang, L. D.; Chen, W.; Meng, G. W.; Zheng, M. J.; Zhao, L. X., Phillipp, F. *Chem. Mater.* **2001**, *13*, 2511.
(8) Zhu, H.; Yang, S.; Ni, G.; Yu, D.; Du, Y. *Scripta Mater.* **2001**, *44*, 2291.
(9) Huang, Y. H.; Okumura, H.; Hadjipanayis, G. C.; Weller, D. *J. Appl. Phys.* **2002**, *91* (10), 6869.
(10) Haruyama, J.; Takesue, I.; Kato, S.; Takazawa, K.; Sato, Y. *Appl. Surf. Sci.* **2001**, *175−176*, 597.
(11) Kawai, S.; Ueda, R. *J. Electrochem. Soc.* **1975**, *122* (1), 32.
(12) Khan, H. R., Petrikowski, K. *J. Magn. Magn. Mater.* **2000**, *215−216*, 526.
(13) Khan, H. R.; Petrikowski, K. *Mater. Sci. Eng.* **2002**, *C 19*, 345.
(14) Furneaux, R. C.; Rigby, W. R.; Davidson, A. P. *Nature* **1989**, *337*, 147.
(15) Masuda, H.; Yanagishita, T.; Yasui, K.; Nishio, K.; Yagi, I.; Rao, T. N.; Fujishima, A. *Adv. Mater.* **2001**, *13* (4), 247.
(16) Doughty, A. S.; Thompson, G. E.; Richardson, J. A.; Wood, G. C. *Trans. Inst. Met. Finish.* **1975**, *53*, 33.
(17) Wada, K.; Hatano, T.; Uchida, K. *J. Appl. Electrochem.* **1979**, *9*, 445.
(18) Wada, K.; Uchida, K. *Adv. Met. Finish. Technol. Jpn.* **1980**, 93.
(19) Kawai, S. *J. Electrochem. Soc.* **1975**, *122* (8), 1026.

10.1021/cm020272w CCC: $22.00 © 2002 American Chemical Society
Published on Web 10/15/2002

the metal is deposited inside the pores during the cathodic half-cycles and is dissolved again during the anodic half-cycles. Because the barrier layer under the porous anodic alumina films functions as a rectifier that preferentially conducts the cathodic current, it results in a net metal deposition.[19] In most cases, the deposits are metallic compounds (valve metal oxide) instead of pure metals and are usually not dense because of the intermittent deposition, thereby limiting the mechanical properties of the deposits. Also, the metals and alloys that can be obtained from the AC electrodeposition are very limited, in addition to the relatively low deposition rate. In contrast, by a direct current (DC) electrodeposition, almost all kinds of metals and alloys can be electrodeposited from various electrolytes, including aqueous solutions to molten salts. In addition, the deposition rate of the DC mode is much higher than that of the AC mode because of the continuous electrodeposition, and the products with good properties can be acquired by the easily controllable process. However, the direct current electrodeposition of metals in the porous anodic alumina films on aluminum is usually impossible because of the insulating nature of the alumina barrier layer. Recently, K. Nielsch et al.[21,22] successfully fabricated the ordered nickel and cobalt nanowire arrays in anodic alumina films on aluminum by a pulsed electrodeposition, by which the nickel or cobalt is deposited in the pores of anodic alumina films via the dendrite pores of the barrier layer formed by a multistep anodization. To the best of our knowledge, however, metal nanowires in porous anodic alumina films on an ITO covered glass has not been successfully produced by a DC electrodeposition.

The purpose of the present study was to fabricate various nanostructure arrays directly on glass substrates using an anodic alumina template by DC electrodeposition. The nanowires fabricated on glass substrates should lead to various applications because of their good mechanical strength, durability against heat treatment at higher temperatures, and optical transparency. In the present paper, we first describe the formation and the microstructures of anodic alumina films (with different pore dimensions) on an ITO-covered glass substrate. A typical ferromagnetic material, nickel, was then electrodeposited (in a DC mode) in the pores of anodic alumina films to obtain Ni nanowire arrays with different aspect ratios. To demonstrate a potential practical application, the changes of magnetization curves of the Ni nanowires depending on the morphology of the nanowires were also investigated.

Experimental Section

Specimens and Solutions. A highly pure aluminum layer (99.99%, ≈1.5 μm), which was deposited on a fluorine-free glass substrate (25 × 100 × 0.7 mm) coated with a tin-doped indium oxide (ITO: ≈130 nm, ≈10 Ω/□) film, was used as the starting sample. Aluminum deposition was performed by RF sputtering in a multi-cycled mode at a rate of 1.5 nm/s.[23,24]

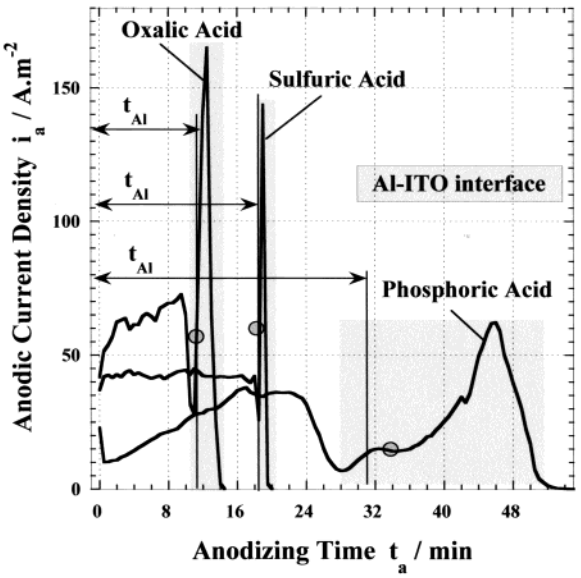

Figure 1. Changes of current density (i_a) with anodization time (t_a) for sputtered aluminum films on glass with an ITO film in solutions of 10% phosphoric acid (130 V, 7 °C), 3% oxalic acid (40 V, 20 °C), and 10% sulfuric acid (15 V, 10 °C).

All the solutions were prepared with analytical-grade reagents and distilled water. Three kinds of solutions (10% (vol) phosphoric acid, 3% (wt) oxalic acid, and 10% (vol) sulfuric acid) were used in aluminum anodization. The electrolyte used for the Ni electrodeposition was composed of 0.38 M $NiSO_4$, 0.13 M $NiCl_2$, 0.65 M H_3BO_4, and 60 ppm $CH_3(CH_2)_{11}OSO_3$-Na, adjusted to pH 5.2 with a 20% NaOH solution.

Fabrication of Nanostructures. The specimens were first degreased by ultrasonic-cleaning in acetone for 10 min and then anodized potentiostatically in solutions of phosphoric (130 V, 7 °C), oxalic (40 V, 20 °C), or sulfuric (15 V, 10 °C) acid, to obtain porous alumina films with different porosities and dimensions. The anodizing conditions were determined by a series of preliminary experiments to achieve the alumina films with the pores perpendicular to the substrates. To avoid repetition, the anodic oxide films formed in phosphoric, oxalic, and sulfuric acid solutions are denoted as phosphoric films, oxalic films, and sulfuric films, respectively. After anodization, the specimens were immersed in a 5% phosphoric acid solution at 30 °C for 2−15 min to remove the insulative alumina barrier layer and expose the conductive ITO film to the electrolyte. Nickel electrodeposition was performed at 1.0−1.5 V and 30 °C for 2−10 min, with magnetic stirring. A pure nickel plate (40 × 120 × 2 mm) was used as the counter electrode. Prior to the Ni electrodeposition, the specimens were immersed in distilled water and treated in an ultrasonic bath for 1 min to eliminate the air in the pores of anodic alumina films. During the anodization and electrodeposition, the variations of current and voltage were monitored by two multi-meters connected with a programmed computer system.

Characterizations. The morphology of the anodized and electrodeposited specimens was investigated by a field emission scanning electron microscope (FESEM, S-5000, Hitachi) with an energy-dispersive X-ray analyzer (EDXA). To minimize charging effects, the specimen was covered with a thin evaporated osmium layer before imaging. The transmittance spectra of the specimens after anodization were measured by a spectrometer (U-3500, Hitachi). The crystallographic structures of the specimens were analyzed by an X-ray diffractometer (XRD, RINT-2000/PC, Cu Ka, 40 V/40 mA) and the structural characterization of the free nanowires was carried out by a transmission electron microscopy (TEM, JEM-1010,

(20) Paulus, P. M.; Luis, F.; Kröll, Schmid, G.; de Jongh, L. J. *J. Magn. Magn. Mater.* **2001**, *224*, 180.
(21) Nielsch, K.; Wehrspohn, R. B.; Barthel, J.; Kirschner, J.; Gösele, U.; Fisher, S. F.; Kronmüller, H. *Appl. Phys. Lett.* **2001**, *79* (9), 1360.
(22) Nielsch, K.; Müller, F.; Li, A.-P.; Gösele, U. *Adv. Mater.* **2000**, *12* (8), 582.
(23) Chu, S. Z.; Wada, K.; Inoue, S.; Todoroki, S. *Chem. Mater.* **2002**, *14*, 266.
(24) Chu, S. Z.; Wada, K.; Inoue, S.; Todoroki, S. *J. Electrochem. Soc.* **2002**, *149* (7), B321.

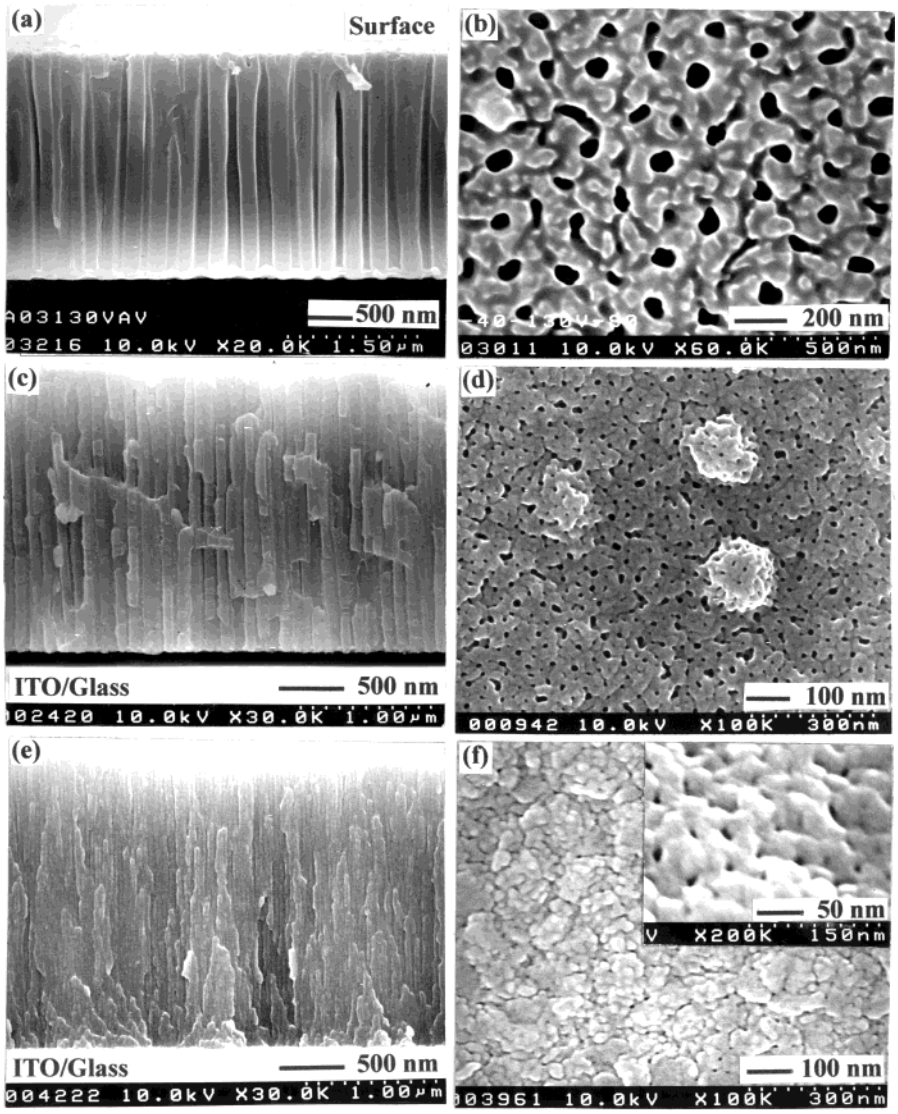

Figure 2. FESEM images of vertical fracture sections and surface morphology for specimens anodized down to the ITO/glass substrate in solutions of (a) and (b) phosphoric acid, $t_a = 35$ min, (c) and (d) oxalic acid, $t_a = 15$ min, and (e) and (f) sulfuric acid, $t_a = 25$ min. Insert in image (f) is the transverse fracture section of (e). Other conditions of anodization are the same as those in Figure 1.

100 kV) following dissolution of anodic alumina in a 5% NaOH solution. Magnetization curves were measured by a vibrating sample Magnetameter (USM, Lake Shore model 7300).

Results and Discussion

Aluminum Anodization on ITO/Glass. Figure 1 shows the time variation in current density ($i_a - t_a$) for the sputtered aluminum specimens anodized in different solutions. For all the specimens, the current density in the $i_a - t_a$ curves exhibits a relatively stable stage, which corresponds to the aluminum layer, and a fluctuating stage, which corresponds to the Al−ITO interface, and finally goes to zero. The anodic current density of the aluminum layers, i_a, is the highest in the oxalic solution, and then the sulfuric solution, and the lowest in the phosphoric solution, irrespective of the applied voltages and the concentrations of the solutions. In particular, the i_a corresponding to the Al−ITO interface exhibits a characteristic swing (see shadow regions), accompanied by gas evolution and sparking phenomena. Meanwhile, the appearance of the specimens also changes from opaque to transparent gradually, indicating the consumption of aluminum. According to our previous studies,[24] the current variation at the interface is ascribed to the anodic reactions (e.g., oxygen evolution from the electrolyte) on the ITO film and/or the anodization of the ITO film, which eventually results in the degradation in conductivity and the locally anodic dissolution of the ITO film. Therefore, to preserve the conductivity of the specimens, in our later experiments, anodization was stopped immediately as the characteristic current variation and transparence were observed (refer to the circle points).

Microstructures of Anodic Alumina Films. The surface and fracture section morphology of the specimens anodized down to the ITO/glass substrates in different acid solutions are shown in Figure 2. For all the specimens, porous alumina structures with straight and parallel channels perpendicular to the substrate are acquired under the given conditions. The pores in the anodic films distribute uniformly throughout the layers, with smaller diameters on the surface than in the inside

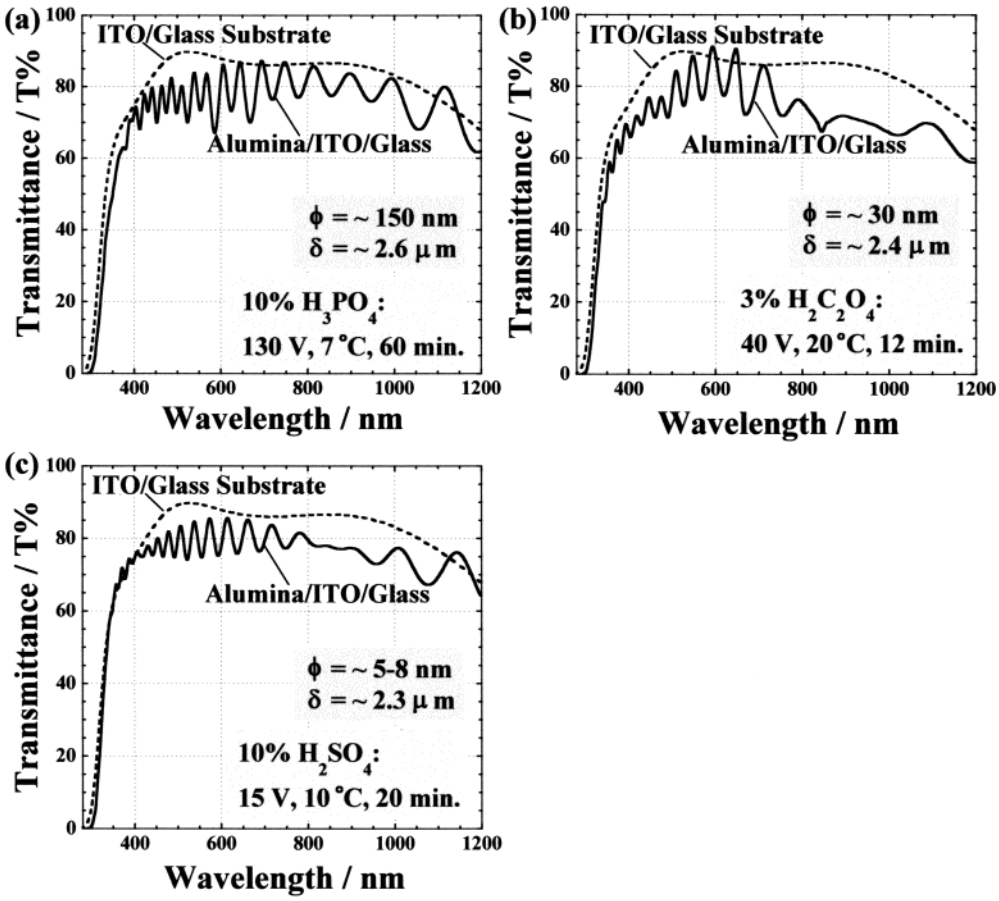

Figure 3. Transmittance spectra for the specimens anodized in different acid solutions. The anodizing conditions are the same as those in Figures 1 and 2.

of the films. The average pore sizes and the pore interspaces at the inside anodic films are approximately 150 and 320 nm, 30 and 110 nm, and 5−8 and 45 nm for the phosphoric, oxalic, and sulfuric films, respectively, basically proportional to the applied voltages. Whereas the average thickness of the three anodic films is 2.6 μm, 2.4 μm, and 2.3 μm, respectively, is possibly correlated to the chemical dissolution in the solutions at the applied temperatures. Noticeably, the resultant alumina films have an arched barrier layer with a thin thickness that is only $^1/_4$−$^1/_3$ of the pore walls (refer to Figures 2a and 2c), which could be caused by the local increases of temperature and/or acidity at the pore bases during the anodization at the Al−ITO interface.[24] The feature of the thin barrier layer of anodic alumina films on the ITO/glass substrates is of significant meaning in our approach because it enables the barrier layer to be selectively removed while preserving the porous alumina nanostructures on the substrates.

Transparency of Anodic Alumina Films on ITO/Glass. The completely anodized specimens are transparent owing to the transparency of the ITO film and the porous structures of anodic alumina films. Figure 3 shows the transmission spectra for the specimens anodized in the different solutions. The average transmittances of the anodic alumina films are close to that of the ITO/glass substrate (dotted line), indicating the transparency of the alumina films throughout the ultraviolet−infrared range. The interference patterns in the spectra could be ascribed to the porosity and the thickness of anodic alumina films, as well as the

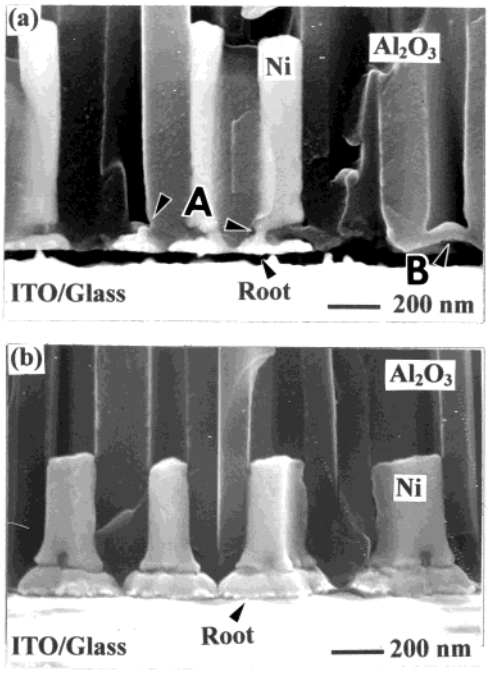

Figure 4. Nickel electrodeposits in the phosphoric anodic alumina films without (a) and after removing (b) the barrier layer.

compositions of the anodic alumina films that usually include some anions from the solutions (PO_4^{3-}, $C_2O_4^{2-}$, or SO_4^{2-}).[25] In our study, the transparency of the anodized specimens is utilized as an important indicator

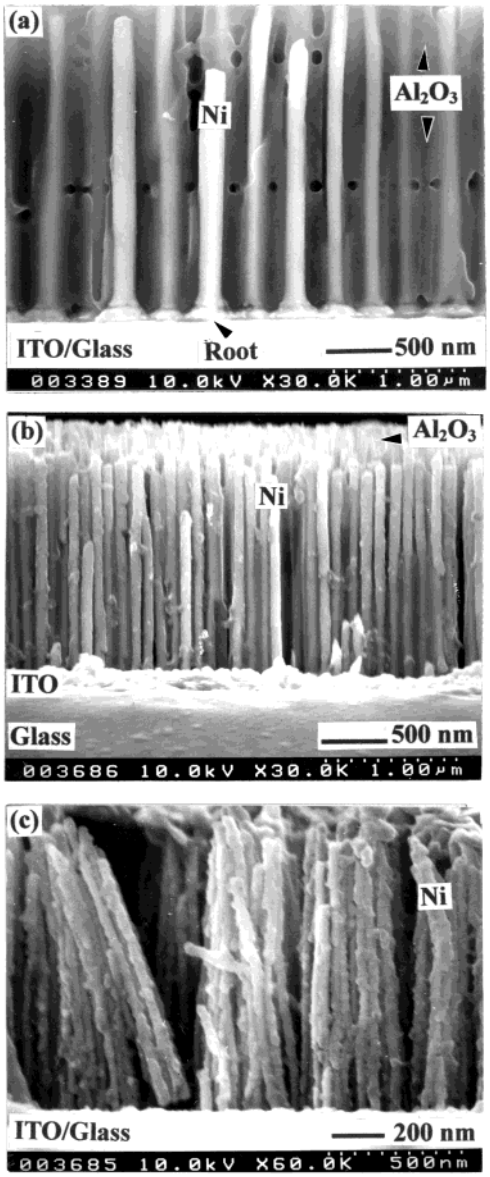

Figure 5. Nickel nanowire arrays standing on ITO/glass substrate in anodic alumina films formed in (a) phosphoric acid, (b) oxalic acid, and (c) sulfuric acid solutions. The average diameters and lengths of the nanowires are ∅ 180 nm and 2.5 μm, ∅ 50 nm and 1.8 μm, and ∅ 18 nm and 1.2 μm, respectively. To show nickel nanowire array clearly, the electrodeposited specimens were etched in a solution of 10% NaOH at room temperature for 10 s−1 min.

to judge the completion of aluminum anodization and to monitor the progressing of the subsequent nickel electrodeposition.

Nickel Electrodeposition in Porous Alumina Films on ITO/Glass. Ni electrodeposition was first attempted on the as-anodized specimens. Astonishingly, Ni electrodeposition occurred directly in the pores of as-anodized alumina films, which is usually impossible for the porous alumina films formed on aluminum sheets because the alumina barrier layer is insulative. Figure 4a gives an example of nickel electrodeposition on the as-anodized specimens formed in the phosphoric acid solution. Nickel electrodeposition starts at the ITO surface and continues in the pores of the porous alumina films via the pinholes on the barrier layer (see arrows A). According to our previous study,[24] the formation of

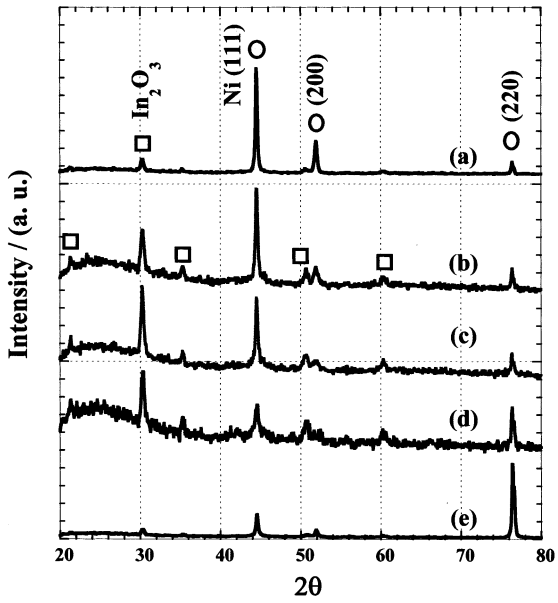

Figure 6. X-ray diffraction patterns of (a) 2-μm Ni film, Ni nanowire arrays embedded in the porous alumina films obtained from (b) phosphoric ∅ 180 nm, (c) oxalic ∅ 50 nm, (d) sulfuric acid solutions ∅ 18 nm, and (e) composite Ni film (1 μm)/nanowires (∅ 18 nm) layer on ITO/glass substrates.

the pinholes on the barrier layers of anodic alumina films on ITO-covered glass may be ascribed to the locally anodic dissolution of the barrier layer and/or the gas evolution during anodization at the Al−ITO interface (Figure 1). Because of the random distribution of the pinholes on the barrier layer, nickel electrodeposition on as-anodized specimens is not uniform. No nickel deposition occurs in the pores without any defect on the barrier layer (see arrow B). Therefore, to achieve uniform Ni deposition in the pores of the films, the insulating barrier layer was removed selectively through a chemical etching to expose the conductive ITO film to the electrolyte. Figure 4b shows a fracture section of nickel columns embedded in the pores of the anodic oxide films after the barrier layer is removed. The Ni columns fill in the pores of the films uniformly and connect directly on the ITO/glass substrate with broad roots that would lead to good adhesion to the substrate. Moreover, it is also found that the remnant conductivity of the ITO film for the anodized specimens plays an important role in nickel electrodeposition in the porous alumina films on ITO/glass substrates. For the specimens anodized down to the ITO film, that is, till the anodic current goes to zero as shown in Figure 1, no nickel electrodeposition occurred even after the insulating barrier layer was removed. [It is found that the conductivity of the bare ITO film on glass without sputtering aluminum changes greatly with anodization in the acidic solutions. During anodization, the anodic current first experienced a sharp increase (300−500 A/m^2) and then went to zero swiftly, lasting only a few seconds. After anodization, the ITO film still exists on the glass substrate but gives a large sheet resistance in several thousands ohms.]

Figure 5 displays various Ni nanowire arrays, with different aspect ratios, partly embedded in the anodic films. The nickel nanowires possesses uniform diameters upright same as the pores. Almost all of the pores are uniformly filled with nickel, according to the SEM

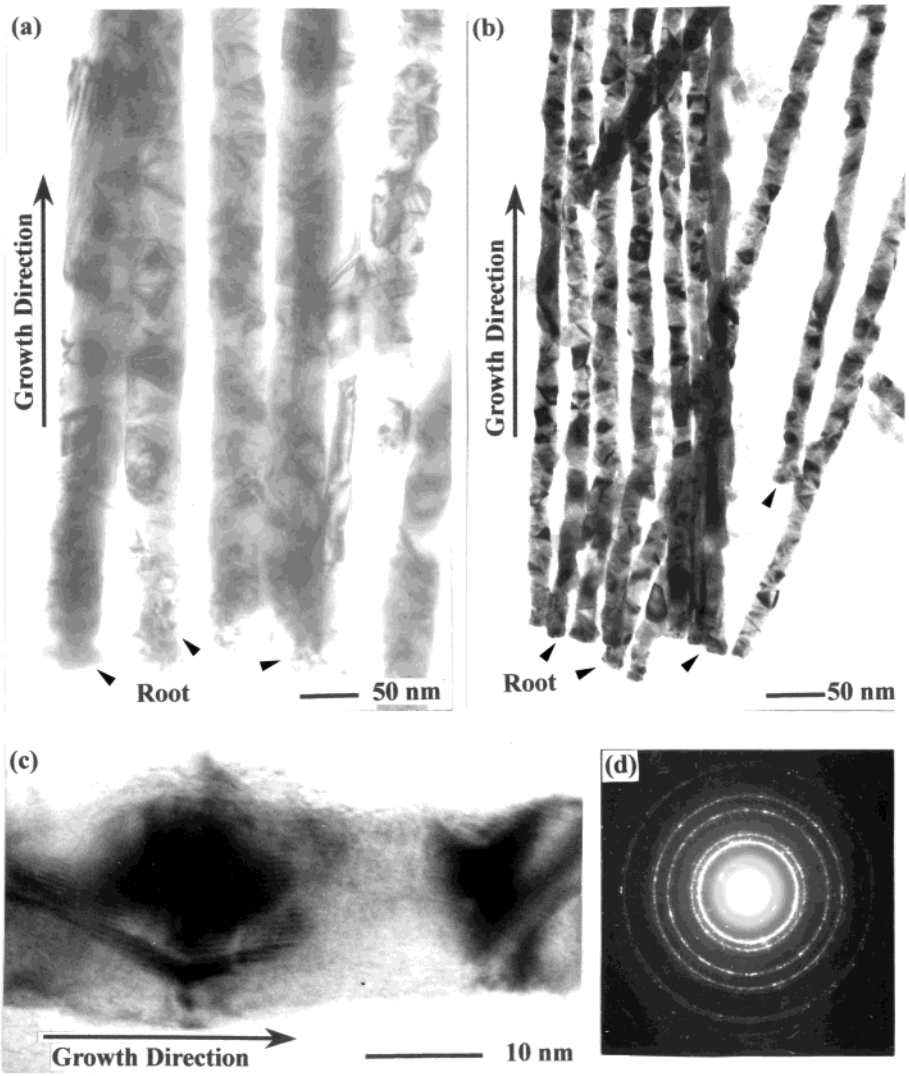

Figure 7. Transmission electron microscopic (TEM) images of the free Ni nanowires fabricated from the anodic alumina films formed in (a) oxalic acid; and (b) and (c) sulfuric acid solution; and (d) the corresponding electron diffraction pattern of (b).

observation of the surface morphology (not shown). The Ni nanowires formed in the phosphoric (5a) and oxalic films (5b) are dense with a smooth surface, whereas the nanowires formed in the sulfuric films (5c) exhibit a chainlike morphology, which would reflect the porous contour of the sulfuric film and/or dimensions of sputtered aluminum particles. The average diameters of the Ni nanowires are 180, 50, and 18 nm for the anodic films formed in phosphoric, oxalic, and sulfuric acid solutions, respectively. On the basis of the film thickness of the three anodic films (Figure 2), the possible maximum aspect ratios of the resultant Ni nanowires are calculated as 14, 48, and 127, respectively.

Crystallographic Structures of Ni Nanowires. It is very interesting that the pore sizes of the anodic oxide films not only define the dimension of the Ni nanowires but also affect the crystal orientation and the grain sizes of the Ni nanowires. Figure 6 gives the X-ray diffraction patterns of the Ni flat film deposited on the ITO/glass substrate (a) and the Ni nanowires embedded in the anodic alumina films (b−e). The Ni nanowires obtained from the phosphoric (b, ∅ 180 nm) and oxalic films (c, ∅ 50 nm) have a polycrystalline fcc structure with a {111} diffraction peak as strong as that of the flat Ni film (a).[26] Whereas the nanowires obtained from the sulfuric films (d, ∅ 18 nm) exhibit a nearly equal intensity of {111} and {220} reflections in the pattern, indicating that the {220} texture has been developed in the Ni nanowires, that is, parallel to the axis of the nanowires. On that basis of the calculated results of integral intensity, I_{111}/I_{220}, the crystal orientation of Ni deposits changes from the {111} texture of the flat film ($I_{111}/I_{220} = 24$) to the {220} texture of nanowires with a lateral dimension of ∅ 18 nm ($I_{111}/I_{220} = 0.96$). More interestingly, the {220} texture of the ∅ 18-nm nanowires is preserved and even enhanced as Ni deposits emerge beyond the surface of the anodic film and form a continuous layer ≈1 μm thick (pattern e, $I_{111}/I_{220} = 0.09$). Moreover, on the basis of the calculation from the Scherrer formula[27] [$0.9\lambda/\beta \cos\theta$; where β = fwhm of the {220} reflection and $\lambda = 1.5405$ Å.], the average sizes of the Ni crystallites perpendicular to the substrate planes are estimated as approximately143 nm (a), 37 nm (b), 35 nm (c), 31 nm (d), and 48 nm (e), respectively.

(25) Takahashi, H.; Fujimoto, K.; Konno, H.; Nagayama, M. *J. Electrochem. Soc.* **1984**, *131*, 1856.
(26) Saitou, M.; Makabe, A.; Tomoyase, T. *Surf. Sci.* **2000**, *459*, L462.
(27) Scherrer, P. Nachr. Göttinger Gesell. *Zwigmondys Kolloidchemie*, 3rd ed., 1918; Vol. 98, p 394.

This indicates that the porous alumina templates also affect the orientation and the dimension of the Ni crystallites in nanowires. Particularly, the crystal dimension of ∅ 18 nm Ni nanowires is much larger in the direction parallel to the axis of the nanowires, indicating that the porous film with small pore size promotes the growth of nickel crystallites in the *Z*-axis direction.

Transmission Electron Micrograph (TEM) Observation. Figure 7 shows the representative TEM images of the free Ni nanowires formed in (a) oxalic and (b) sulfuric acid films. The Ni nanowires, with average diameters of 50 and 18 nm, are composed of tetrahedral crystalline grains with dimensions equivalent to the pore sizes of the anodic alumina templates, indicating that the crystal growth in the Ni nanowires is defined by the pore walls. It should be noted that the morphology of the Ni nanowires achieved in the present method is significantly different from that formed by an AC electrodeposition, by which the granularity of Ni deposits is usually much smaller than the pore of the anodic films because of the intermittent deposition.[10,17−19] Figures 7a and 7b also display the roots of the nanowires (see arrows), which were originally connected to the ITO substrate. The Ni nanowires near their roots consist of numerous Ni crystallites that are much smaller than those in the other parts of the nanowires. This structural feature of the Ni nanowires, which is reported by the present study for the first time, may be ascribed to the nucleation and growth process of Ni crystallites deposited on the foreign substrate, that is, the ITO substrate.[28] The fact that the nickel crystal grains near the roots are smaller than those of the other parts of the wires may infer that the Gibbs formation energy of nickel nucleation on the ITO film is smaller than that of the nickel growth (refer to Figure 4a).[28] The small granularity of Ni nanowires near their roots means that the anodized ITO film benefits the nucleation of nickel in electrodeposition. In other words, the anodized ITO film is active or conductive enough to induce the nucleation of nickel in electrodeposition without additional special treatment prior to electrodeposition.

Figure 7c gives a high-resolution transmission electron micrograph (HRTEM) image of the ∅ 18-nm nanowires. It shows clearly that the tetrahedral nickel crystals are connected by the amorphous grain boundary with smaller diameters than the grains, which is reflected as a chainlike morphology of the Ni nanowires shown in Figure 5c. The crystal grain of the nanowires is ≈20 nm along the axis of the nanowires, which is consistent with the result calculated from the Scherrer formula. A typical diffraction pattern (Figure 7d) taken from the bundle of the Ni nanowires (∅ 18 nm) in Figure 7b shows several continuous rings, indicating that the Ni nanowires are highly crystalline and have a polycrystalline structure. Moreover, the diffraction patterns of the Ni nanowires formed in the oxalic (∅ 50 nm) and phosphoric (∅ 180 nm) films are similar to that in the sulfuric films (∅ 18 nm) and the crystalline morphology of the ∅ 180-nm nanowires could not be observed because of the large diameter of the wires.

Magnetization Characteristics of Ni Nanowire Arrays on Glass. Because nickel is a ferromagnetic material, one of the most promising applications of the Ni nanowire arrays would be micromagnetic devices such as high-density recording media.[2−13,21] For instance, Niesch et al. reported that the coercivity of the Ni nanowires embedded in porous alumina films on aluminum sheets increased to 1200 Oe as the diameter of the Ni columns decreased to 30 nm.[21] Figure 8 shows the magnetic hysteresis loops of various Ni nanowire arrays embedded in the anodic alumina films with different dimensions. For Ni nanocolumns with aspect ratio 3 (a), the easy axis of magnetization is parallel to the film plane or perpendicular to the nanocolumns, while for the Ni nanowires (b) and (c), the easy axis of magnetization is perpendicular to the film plane and parallel to the nanowires. This indicates that the easy axis of magnetization changes from in-plane to perpendicular direction with increasing aspect ratio of the nanowires. This magnetic anisotropy originates from the shape anisotropy of the nanowires with high aspect ratios. The anisotropy field (H_k) of the nanowires (b) and (c) is ≈ 3 kOe, which is close to the theoretical value estimated for the spheroid with a large aspect ratio, that is, 2πMs ≈ 3 kOe. The values of coercivity (H_c) and squareness (M_r/M_s) for various Ni nanostructures are summarized in Table 1. The M_r/M_s values of the nanowires, which are usually considered an important parameter in magnetic recording media, are proportional to the aspect ratios of the nanowires, showing the

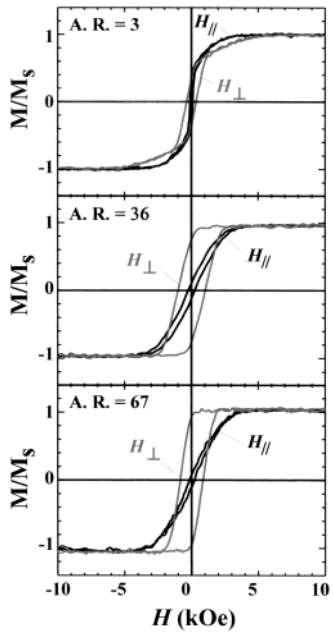

Figure 8. Magnetization hysteresis loops of various Ni nanowire arrays on an ITO/glass substrate embedded in anodic alumina films formed in (a) phosphoric, (b) oxalic, and (c) sulfuric acid solutions. The average diameters and the nearest neighbor distances of the nanowires are approximately ∅ 180 and 140 nm, ∅ 50 and 10 nm, and ∅ 18 and 27 nm, respectively.

Table 1. Magnetization Characteristics of Various Ni Nanowire Arrays on ITO/Glass Substrate

Ni nanowires (diameter, length)	aspect ratio (L/D)	H_c (Oe)		M_r/M_s	
		⊥	//	⊥	//
(a) ∅ 180 nm, 0.5 μm	3	362.5	100.0	0.35	0.36
(b) ∅ 50 nm, 1.8 μm	36	**1025.0**	100.9	**0.74**	0.12
(c) ∅ 18 nm, 1.2 μm	67	**830.5**	200.0	**0.94**	0.09

(28) Budevski, E.; Staikov, G.; Lorenz, W. J. *Electrochim. Acta* **2000**, *45*, 2559.

highest value of 0.94 for nanowires (c) with a diameter of ∅ 18 nm and the largest aspect ratio of ≈67. The coercivity (H_c), on the other hand, exhibits the highest value of 1025.0 Oe for the nanowires (b) with a larger diameter of ∅ 50 nm and a smaller aspect ratio of 36. Because the shape anisotropy field coefficient of spheroids is 6 with aspect ratios larger than 10, nanowires (b) and (c) are expected to have similar shape anisotropy. Thus, the coercivity difference in nanowires (b) and (c) is thought to be caused by some other factor(s) such as the orientation of individual grains within a nanowire and/or the local morphological change of the nanowires.

Conclusions

We have successfully fabricated various ordered Ni nanowire arrays on glass substrates by a combined technique of aluminum anodization and a conventional DC electrodeposition. To the best of our knowledge, this is the first example of preparation of ordered metal nanostructure arrays on glass substrate with an ITO film. The pore sizes of the template electrodes of the anodic alumina films can be controlled by anodization and chemical dissolution, which define the diameter and the crystal orientation of the nanowires. The Ni nanowire arrays with high aspect ratios exhibit an anisotropy perpindicular to the film plane, inferring a promising future for application to magnetic recording media. More significantly, by utilizing various sophisticated DC electrodepositing processes, the present approach may be used to fabricate various nanostructure arrays, not only metals but also oxides or semiconductors, in porous alumina films on glass for various applications.

Acknowledgment. This work is part of the Japan Millennium Project of Exploration and Creation of a Catalyst for Removing Harmful Chemical Substances. We thank The Asahi Glass Co., Ltd., for providing glass substrates with ITO films and Kyodo International Company for producing sputtered aluminum. We also thank K. Kurashima for assisting in TEM observation.

CM020272W